

Impact of Ly α radiation force on super-Eddington accretion onto a massive black hole

Takuya MUSHANO¹, Takumi OGAWA^{1,*}, Ken OHSUGA¹, Hidenobu YAJIMA¹, and Kazuyuki OMUKAI²

¹Center for Computational Sciences, University of Tsukuba, Ten-nodai, Tsukuba, Japan

²Astronomical Institute, Graduate School of Science, Tohoku University, Sendai, Japan

*E-mail: takumi@ccs.tsukuba.ac.jp

October 8, 2024

Abstract

The viability of super-Eddington accretion remains a topic of intense debate, crucial for understanding the formation of supermassive black holes in the early universe. However, the impact of Ly α radiation force on this issue remains poorly understood. We investigate the propagation of the Ly α photons and evaluate the Ly α radiation force within a spherically symmetric accreting HI gas onto the central black hole. We solve the radiation transfer equation, incorporating the destruction processes of Ly α photons through two-photon decay and collisional de-excitation. We find that the Ly α photons, originating in the HII region around black holes, suffer from multiple resonance scattering before being destroyed via two-photon decay and collisional de-excitation. Hence, the Ly α radiation force undergoes a significant amplification, surpassing gravity at the innermost section of the HI region. This amplification, quantified as the force multiplier, reaches approximately 130 and remains nearly constant, regardless of the optical depth at the line center, provided the optical thickness of the flow is within the range of 10^{10-14} . The requisite lower limit of the product of gas density and black hole mass to realize the super-Eddington accretion is found to be in the range $(2 - 40) \times 10^9 M_{\odot} \text{cm}^{-3}$, which is a few to tens of times larger than the minimum value obtained without accounting for the Ly α radiation force. The pronounced amplification of the Ly α radiation force poses a substantial challenge to the feasibility of super-Eddington accretion.

Key words: radiative transfer — black hole physics — quasars: supermassive black holes — cosmology: theory

1 Introduction

Supermassive black holes (hereafter, SMBHs) ubiquitously exist at the centers of large galaxies. The tight correlation of their masses with those of host galaxies strongly suggests their coevolution (Kormendy & Ho, 2013, for the review). Despite decades of intensive investigations into the origin of those SMBHs, it still remains as one of the most significant enigmas in astrophysics. The discoveries of SMBHs in the early universe (Fan et al., 2004; Mortlock et al., 2011; Wu et al., 2015; Matsuoka et al., 2018; Bogdán et al., 2024) provide very strong constraints on the timescale of their growth. While various hypotheses exist regarding the formation of SMBHs (Volonteri, 2012; Haiman, 2013; Inayoshi et al., 2020, for the review), the super-Eddington growth of seed black holes (BHs) in massive, dense atomic gas clouds emerges as one of the most promising scenarios.

Super-Eddington accretion flow has been investigated by a number of authors. Within the scale extending from the event horizon to the centrifugal radius, an accretion disk forms around a BH. At this scale, super-Eddington accretion occurs naturally in environments characterized by abundant gas supply, driven by

the interplay of photon trapping and the anisotropy of radiation (Watarai et al. 2000; Ohsuga et al. 2005; McKinney et al. 2014; Jiang et al. 2014; Sądowski et al. 2015; and Ohsuga & Mineshige 2014 for the concise review).

On larger scales, comparable to the Bondi radius, the situation differs significantly. The radiation originating from the vicinity of the central black hole is expected to be approximately spherically symmetric, primarily due to electron scattering, ionization, and recombination processes. Although some anisotropy may exist around the black hole, the mechanical forces are also spherically symmetric, as the centrifugal force becomes nearly negligible in regions far from the centrifugal radius. Therefore, instead of disk accretion, a roughly spherical accretion flow is realized, leading to a more pronounced influence of radiation pressure and heating on the accretion dynamics. A number of investigations by different authors have confirmed that accretion rates in such flows are significantly lower than the Eddington rate (Milosavljević et al. 2009a,b; Park & Ricotti 2011, 2012, 2013). Later, Inayoshi et al. (2016), performing one-dimensional spherically symmetric radiation hydrodynamic simulations incorporating photo-ionization from the Bondi scale down to the photon

trapping radius, reported that the accretion rate becomes comparable to the Bondi rate, which as large as thousands of times the Eddington rate, provided the condition $n_\infty M_{\text{BH}} > 10^9 M_\odot \text{cm}^{-3}$ is satisfied. Here n_∞ is the gas density at the infinity and M_{BH} is the BH mass. This condition is determined by the comparison between the sizes of the Strömgen and Bondi radii.

Their results are particularly noteworthy as they reveal the possibility of super-Eddington accretion even under the most conservative assumption of spherical accretion. Several authors also investigated the condition under which super-Eddington accretion is realized in this context (Sakurai et al., 2016; Yajima et al., 2017; Takeo et al., 2018; Sugimura et al., 2017; Toyouchi et al., 2021). They report that radiation pressure is rather subdominant and radiation mainly affects dynamics via photo-ionization heating of the inflowing gas, by taking into account the electron scattering and the bound-free absorption of the primordial gas in estimating the radiation force. However, the pressure of Ly α photons, generated through the recombination of hydrogen atoms, may impact gas dynamics significantly as it is amplified by multiple resonance scatterings (Milosavljević et al., 2009a; Smith et al., 2015). The Ly α radiation force increases with the increase of the typical optical depth of a system (Adams 1975; Smith et al. 2016; Dijkstra et al. 2006 and Dijkstra 2019 for the review). For example, in a massive halo with the line-center optical depth of 10^{11} and a temperature of 10^4 K, the force can be amplified by 10^3 times compared to the single-scattering case.

The destruction process of Ly α photons, such as the two-photon decay and the collisional de-excitation, can be important in the context of the super-Eddington growth of massive seeds. Although the two-photon decay is a forbidden transition from the 2s to 1s levels of atomic hydrogen and its probability is much smaller than that of resonant scattering, it becomes significant in highly optically thick media. This is because the Ly α photon undergoes numerous scatterings before escaping to the outside. The decrease in the number of Ly α photons due to collisional de-excitation is also non-negligible in dense media.

In this paper we investigate the effect of Ly α radiation on the Bondi accretion flows onto intermediate-mass black holes under fixed gas properties, such as density, velocity and temperature. We solve the Ly α radiative transfer by employing the radiation diffusion and Fokker-Planck approximations (Neufeld, 1990). We consider the destruction mechanisms of the Ly α photons by the two-photon decay and the collisional de-excitation, and compare the radiation force to the gravity to estimate whether super-Eddington accretion is feasible or not.

This paper is organized as follows: In Section 2, we introduce the basic equations and assumptions of our models. Section 3 presents our results and discusses the feasibility of super-Eddington accretion, and finally in Section 4, we summarize our study.

2 Basic Equations and Numerical Methods

We suppose a spherical accretion flow of pure hydrogen gas onto a BH at the center. Surrounding the BH, there should be a spherical HII region, extending sufficiently far from the BH, created by

the ionizing photons emitted from the circum-BH accretion disk. Enormous Ly α photons are emitted outward from the HII region and then undergo multiple scattering by purely atomic hydrogen gas. Hence we set the innermost region of our simulation domain to correspond to the outermost region of the HII region.

We assume that the flow within the domain follows a spherically symmetric isothermal Bondi accretion pattern with the typical temperature of atomic cooling halos (10^4 K), emulating the super-Eddington flow demonstrated in Inayoshi et al. (2016). By fixing the distribution of fluid variables, such as fluid velocity, density, and temperature, based on the super-Eddington isothermal Bondi accretion of purely atomic hydrogen gas onto a central black hole, we investigate the steady distributions of Ly α photons. Additionally, we assess the radiation force resulting from the resonance scattering of Ly α photons. Given that the Ly α radiation from the innermost region (i.e. the HII region) originates from the BH accretion disk, the Ly α luminosity should depend on the accretion rate. The details of our calculation setup are described below.

2.1 Basic equations

In order to account for the multiple scattering of Ly α photons in highly optically thick flows, we solve the frequency-dependent 0-th moment equation of radiation, in which the radiation diffusion approximation and the Fokker-Planck approximation are employed, with terms up to $O(v/c)$ being taken into account. Since the photon diffusion time scale is much shorter than the dynamical time in the present situation, the radiation fields can be regarded to become immediately steady. Applying these approximations and assumptions to Eq.(95.18) (95.19) of Mihalas & Mihalas (1984), the basic equation to be solved here is

$$\begin{aligned} & -\frac{1}{r^2} \frac{\partial}{\partial r} \left(\frac{cr^2}{3\kappa_{x_0}} \frac{\partial E_{x_0}}{\partial r} \right) \\ & + \frac{1}{r^2} \frac{\partial}{\partial r} (r^2 v E_{x_0}) + \frac{1}{r^2} \frac{\partial}{\partial r} (r^2 v) \frac{1}{3} E_{x_0} \\ & - \frac{1}{r^2} \frac{\partial}{\partial r} (r^2 v) \frac{\partial}{\partial x_0} \left[\left(\frac{c}{v_{\text{th}}} + x_0 \right) \frac{1}{3} E_{x_0} \right] \\ & = -\kappa_{x_0}^a c E_{x_0} + 4\pi \eta_{x_0}^r + \frac{1}{2} \frac{\partial}{\partial x_0} \left(c \kappa_{x_0}^s \frac{\partial E_{x_0}}{\partial x_0} \right), \end{aligned} \quad (1)$$

where r , c , v and v_{th} are the distance from the origin (BH), the speed of light, the fluid velocity and the thermal velocity in the gas, respectively. The normalized frequency x_0 is defined as $x_0 = (\nu_0 - \nu_\alpha)/\Delta\nu_D$, where ν_0 , ν_α and $\Delta\nu_D$ are the frequency of photons in the fluid comoving frame, the frequency at the Ly α line center, $\nu_\alpha = 2.466 \times 10^{15}$ Hz, and the typical Doppler shift by the thermal motion of gas around the Ly α line, $\Delta\nu_D = v_{\text{th}} \nu_\alpha / c$, respectively. $\kappa_{x_0}^a$, $\kappa_{x_0}^s$, κ_{x_0} and $\eta_{x_0}^r$ are the absorption coefficient related to the two-photon decay and the collisional de-excitation, the scattering coefficient of the resonance scattering, the total opacity defined by $\kappa_{x_0} = \kappa_{x_0}^s + \kappa_{x_0}^a$ and the emission coefficient, respectively, all of which are measured in the fluid comoving frame and at normalized frequency of x_0 . The radiation energy density E_{x_0} is defined in the comoving frame as $E_{x_0} \equiv \int \frac{1}{c} I_{x_0} d\Omega_0$ where I_{x_0} is the intensity in the comoving frame at the frequency

x_0 , where Ω_0 is the solid angle measured in the comoving frame. Eq.1 includes effects related to the fluid velocity, such as trapping effects by the inflowing medium, the work from/to fluid and the Doppler effects by the velocity dispersion, which correspond to the second, third and fourth terms of the left-hand side, respectively.

The scattering coefficient for the pure resonant scattering, $\bar{\kappa}_{x_0}^s$, is defined as $\bar{\kappa}_{x_0}^s \equiv \sigma_0 H(a, x_0) n_{\text{HI}}$ where σ_0 , $H(a, x_0)$ and n_{HI} are the cross-section at the Ly α line center, the Voigt function, and the number density of the neutral hydrogen gas, respectively. The cross-section σ_0 and the Voigt function are defined by

$$\sigma_0 = f_{12} \frac{\sqrt{\pi} e^2}{m_e c \Delta \nu_D} \approx 5.88 \times 10^{-14} \left(\frac{T}{10^4 \text{K}} \right)^{-1/2} \text{cm}^2, \quad (2)$$

$$H(a, x) = \frac{a}{\pi} \int_{-\infty}^{\infty} \frac{e^{-y^2}}{(x-y)^2 + a^2} dy, \quad (3)$$

where e , m_e , f_{12} and a are the elementary charge, the electron mass, the oscillator strength, $f_{12} = 0.4162$, and the Voigt parameter, $a = \Delta \nu_L / (2\Delta \nu_D)$, which is the ratio between the natural width $\Delta \nu_L$ and the thermal width of the Ly α line, respectively.

The absorption coefficient $\kappa_{x_0}^a$, due to the two-photon decay and the collisional de-excitation, is written as $\kappa_{x_0}^a = p_{\text{dest}} \bar{\kappa}_{x_0}^s$ where the photon destruction probability p_{dest} is the probability that a Ly α photon is annihilated at a single resonance-scattering. With photon destruction, the scattering coefficient κ^s becomes slightly different from that for pure resonant scattering $\bar{\kappa}^s$ and can be written as $\kappa_{x_0}^s = (1 - p_{\text{dest}}) \bar{\kappa}_{x_0}^s$. Assuming that the hydrogen is in the ground state or in the first excited state and that the higher excited states can be ignored, the photon destruction probability can be calculated as

$$p_{\text{dest}} = \frac{A_{2\text{ph}} + C_{21}}{A_{\text{Ly}\alpha} + A_{2\text{ph}} + C_{21}}. \quad (4)$$

where $A_{\text{Ly}\alpha}$ is the rate of the Ly α production by spontaneous emission, $A_{2\text{ph}}$ is the rate of the two photon decay and C_{21} is the rate of the collisional de-excitation from the first excited state to the ground state, respectively. These rates can be written as

$$A_{\text{Ly}\alpha} = \frac{n_{2\text{p}}}{n_2} A_{2\text{p}1\text{s}} = \frac{1}{1 + r_{2\text{s}2\text{p}}} A_{2\text{p}1\text{s}}, \quad (5)$$

$$A_{2\text{ph}} = \frac{n_{2\text{s}}}{n_2} A_{2\text{s}1\text{s}} = \frac{r_{2\text{s}2\text{p}}}{1 + r_{2\text{s}2\text{p}}} A_{2\text{s}1\text{s}}. \quad (6)$$

where $A_{2\text{p}1\text{s}} = 6.25 \times 10^8 \text{ s}^{-1}$, $A_{2\text{s}1\text{s}} = 8.25 \text{ s}^{-1}$ and $r_{2\text{s}2\text{p}}$ are the Einstein coefficients for the transition $2\text{p} \rightarrow 1\text{s}$, $2\text{s} \rightarrow 1\text{s}$ and the ratio between the number densities in the 2s and the 2p states, respectively. Due to the very short timescale to achieve the equilibrium among the number of particles in the 1s, 2s and 2p states, the transition rates from/into the 2s state can be considered to balance and therefore the ratio $r_{2\text{s}2\text{p}}$ can be calculated as

$$r_{2\text{s}2\text{p}} = \frac{C_{2\text{p}2\text{s}}}{C_{2\text{s}2\text{p}} + A_{2\text{s}1\text{s}}}. \quad (7)$$

where $C_{2\text{s}2\text{p}}$ and $C_{2\text{p}2\text{s}}$ are the rates of the transition $2\text{s} \rightarrow 2\text{p}$ and $2\text{p} \rightarrow 2\text{s}$ by collisions, respectively. They are written as

$$C_{2\text{s}2\text{p}} = 5.31 \times 10^{-4} \left(\frac{n_e}{1 \text{ cm}^{-3}} \right) \text{s}^{-1}, \quad (8)$$

$$C_{2\text{p}2\text{s}} = C_{2\text{s}2\text{p}} \frac{g_{2\text{s}}}{g_{2\text{p}}} = 1.77 \times 10^{-4} \left(\frac{n_e}{1 \text{ cm}^{-3}} \right) \text{s}^{-1}. \quad (9)$$

where $g_{2\text{s}} = 2$ and $g_{2\text{p}} = 6$ are the statistical weight of the 2s state and the 2p state and n_e is the electron number density, respectively (see Seaton 1955).

The rate of the collisional de-excitation (Omukai, 2001; Inayoshi et al., 2016), C_{21} , is given by

$$C_{21} = \gamma_{21}(\text{e}) n_e + \gamma_{21}(\text{H}) n_{\text{H}}, \quad (10)$$

where n_{H} is the hydrogen number density, $\gamma_{21}(\text{e})$ and $\gamma_{21}(\text{H})$ are the de-excitation coefficients for the collisions with electrons and hydrogen atoms, respectively, which are given by substituting $(u, l) = (2, 1)$ into the formulae (Sobel'Man et al., 1995; Drawin, 1969) as below:

$$\gamma_{ul}(\text{e}) = 10^{-8} \left(\frac{l^2}{u^2 - l^2} \right)^{3/2} \frac{l^3}{u^2} \alpha_{lu} \frac{\sqrt{\beta(\beta+1)}}{\beta + \chi_{lu}}, \quad \beta = \frac{h(v_l - v_u)}{kT}, \quad (11)$$

$$\gamma_{ul}(\text{H}) = 7.86 \times 10^{-15} \left(\frac{l}{u} \right)^2 \left(\frac{1}{l^2} - \frac{1}{u^2} \right)^{-2} f_{lu} T^{1/2} \times \frac{1 + 1.27 \times 10^{-5} (1/l^2 - 1/u^2)^{-1} T}{1 + 4.76 \times 10^{-17} (1/l^2 - 1/u^2)^{-2} T^2}. \quad (12)$$

where the coefficients are $\alpha_{12} = 24$ and $\chi_{12} = 0.28$.

2.2 Numerical setup

We solve discretized Eq.1 based on the finite volume method by using the alternating-direction implicit (ADI) method. We set the gas temperature, the ionization degree, the mean molecular weight to be $T = 10^4 \text{K}$, $x_e = n_e/n_{\text{HI}} = 10^{-4}$ and $\mu = 1$, respectively (see also Inayoshi et al. 2016; Sakurai et al. 2016). The profiles of the gas density and velocity are calculated by solving the fluid equation for the Bondi accretion without radiation effects, using the 11 parameter sets of $(n_\infty, M_{\text{BH}})$ (all parameter sets are shown in Table 1 of the model "Bondi") The Bondi accretion rate, \dot{M}_{B} , is given by

$$\dot{M}_{\text{B}} \approx 4 \times 10^3 \left(\frac{L_{\text{Edd}}}{c^2} \right) \left(\frac{M_{\text{BH}}}{10^4 M_\odot} \right) \left(\frac{n_\infty}{10^5 \text{ cm}^{-3}} \right) \left(\frac{T}{10^4 \text{K}} \right)^{-3/2}. \quad (13)$$

where L_{Edd} is the Eddington luminosity for the Thomson scattering.

The total optical depth at the Ly α line center, measured over the radial line of the computational domain, τ_0 , can be approximately written as

$$\tau_0 \approx 4.3 \times 10^{11} \left(\frac{n_\infty}{10^5 \text{ cm}^{-3}} \right) \left(\frac{M_{\text{BH}}}{10^4 M_\odot} \right) \left(\frac{T}{10^4 \text{K}} \right)^{-3/2} \left(\frac{r_{\text{min}}}{10^{-3} r_{\text{B}}} \right)^{-1/2}, \quad (14)$$

assuming that the number density distribution $n(r) \propto r^{-3/2}$ and the outer boundary of the radial integral of $\sigma_0 n(r)$ is set to infinity, where r_{B} is the Bondi radius which depends on M_{BH} , T , and r_{min} which is the innermost radius of the computational domain defined below.

The radii of the inner and outer boundaries of the computational domain are $r_{\min} = 10^{-3}r_B$ and $r_{\max} = 10^{-1}r_B$, respectively. The innermost radius is the same as in Inayoshi et al. (2016); Sakurai et al. (2016). The number of radial grid cells is set to be $N = 800$. The radial grid is set so that the sequence of the radial length of cells becomes the geometrical sequence with the initial value $\Delta r_0 = 10^{-7}r_{\min}$ and the common ratio ϵ . Here, Δr_0 corresponds to the size of the finest (innermost) grid cell and the common ratio $\epsilon \approx 1.02131$ satisfies the equation below:

$$r_{\max} - r_{\min} = \Delta r_0 \frac{\epsilon^N - 1}{\epsilon - 1}. \quad (15)$$

Such a grid design is convenient since we can control the size of the finest grid cell without changing r_{\min} , r_{\max} and N . Note that it is irrelevant that the simulation domain does not include the Bondi radius because both the gravitational and radiation forces at such a distant region are small and their impacts on the flow are negligible (see also Fig.1).

The grid for the normalized frequency spans over the range of $[x_{\min}, x_{\max}]$, where we set $x_{\min} = -2(a\tau_0)^{1/3}$, and $x_{\max} = 5(a\tau_0)^{1/3}$. The grid interval Δx_0 is set to unity within the range $[-10, 10]$, and $\Delta x_0 = (x_{\max} - x_{\min})/100$ otherwise, considering the significant and steep change in the line profile near the line center.

The situation where $\text{Ly}\alpha$ photons are entering the computational domain, passing through the inner boundary at the rate of $L_{\text{Ly}\alpha}$, is reproduced by setting the emissivity at the innermost cell as follows:

$$\eta_{x_0}(r_0) = \frac{L_{\text{Ly}\alpha}}{4\pi} \frac{1}{\Delta V_0} \frac{H(x_0)}{\sqrt{\pi}}. \quad (16)$$

where ΔV_0 is the volume of the innermost cell. The inner boundary condition of the spatial grid is set as the mirror boundary.

Assuming the radiation is isotropic and can leak freely from outer boundary, the outer boundary condition can be described as

$$F_0(r_{\max}, x_0) = \frac{1}{2} c E_0(r_{\max}, x_0). \quad (17)$$

The radiation energy density at the frequency grid boundaries $x_0 = x_{\min}$ and x_{\max} is set to be zero at all radii.

We investigate the two different cases of accretion flow named as the "slim" and "Eddington" cases. In the "slim" case, the $\text{Ly}\alpha$ luminosity is given as

$$L_{\text{Ly}\alpha} = 0.2 \left[1 + \ln \left(\frac{\dot{M}_B c^2}{20 L_{\text{Edd}}} \right) \right] L_{\text{Edd}}, \quad (18)$$

by assuming 10% of the disk luminosity is converted into $\text{Ly}\alpha$ luminosity (Sakurai et al., 2016) and using the disk luminosity of the slim disk model from Watarai et al. (2000). It should be noted that the accretion rate of our models is typically 10^3 times larger than the Eddington limit as seen in Eq.13. In the "Eddington" case, we employ $L_{\text{Ly}\alpha} = 0.1 L_{\text{Edd}}$ (Inayoshi et al., 2016). We will primarily focus on discussing the result of the "slim" case while the "Eddington" case will also be used to compare with the previous studies.

model	$M_{\text{BH}}[M_\odot]$	$n_\infty[\text{cm}^{-3}]$	τ_0	M_F
Bondi	10^4	10^4	4.2×10^{10}	110
Bondi	10^4	10^5	4.2×10^{11}	110
Bondi	10^4	10^6	4.2×10^{12}	120
Bondi	$10^{4.5}$	10^6	1.3×10^{13}	130
Bondi	10^5	10^4	4.2×10^{11}	100
Bondi	10^5	10^5	4.2×10^{12}	120
Bondi	10^5	10^6	4.2×10^{13}	140
Bondi	$10^{5.5}$	10^5	1.3×10^{13}	130
Bondi	10^6	10^4	4.2×10^{12}	140
Bondi	10^6	10^5	4.2×10^{13}	140
Bondi	10^6	10^6	4.2×10^{14}	150
hom. sphere	N/A	10^9	10^{10}	180
hom. sphere	N/A	10^9	10^{11}	180
hom. sphere	N/A	10^9	10^{12}	180
hom. sphere	N/A	10^9	10^{13}	180

Table 1: Model parameters and results. The model parameters \dot{M}_{BH} and n_∞ are the BH mass and the density at infinity, respectively, τ_0 is the total optical depth measured over the computational domain along the radial direction and M_F is the resulting force multiplier. The model name "Bondi" indicates the model where the Bondi-like fluid field is used and "hom. sphere" means the model where the homogeneous and static medium is used and thus the system in this model predominantly depends on the optical depth τ_0 and weakly depends on density n_∞ (see Fig.5 for more detail)

3 Results

3.1 Radial profile of $\text{Ly}\alpha$ radiation force

In Fig.1 we present radial profiles of the $\text{Ly}\alpha$ radiation force per unit volume,

$$f_{\text{rad}} = - \int \frac{1}{3} \frac{\partial E_{x_0}}{\partial r} dx_0, \quad (19)$$

along with gravity for the case with $M_{\text{BH}} = 10^{5.5} M_\odot$ and $n_\infty = 10^5 \text{ cm}^{-3}$ both for the "slim" and "Eddington" cases.

It is found from the figure that the $\text{Ly}\alpha$ radiation force is higher in the "slim" case than in the "Eddington" case since the $\text{Ly}\alpha$ photons are emitted more efficiently in the "slim" case.

In both cases, within the region $r - r_{\min} \lesssim 10^{12} \text{ cm}$, where $r_{\min} \simeq 6.2 \times 10^{16} \text{ cm}$, the radiation force is significantly enhanced due to numerous photon scatterings, exceeding gravity by approximately 10^6 times. However, as the radius increases, the radiation force decreases monotonically and drastically in both cases, falling below gravity for $r - r_{\min} \gtrsim 5 \times 10^{16} \text{ cm}$. This decline is attributed to the two-photon decay process. $\text{Ly}\alpha$ photons are destroyed in the vicinity of the inner boundary since the photon destruction length, which is the distance a photon travels before it is destroyed via the two photon decay, is very small $\sim 10^{12} \text{ cm}$ (see also Eq. 33 in Appendix B). Thus, the number of photons decreases dramatically with increasing $r - r_{\min}$, leading to a reduction in the radiation force.

The observed trend, where the radiation force surpasses gravity in the innermost region and decreases with increasing radius, is consistent across all parameter sets. For computational domains with smaller optical depths, the radius (normalized by the Bondi

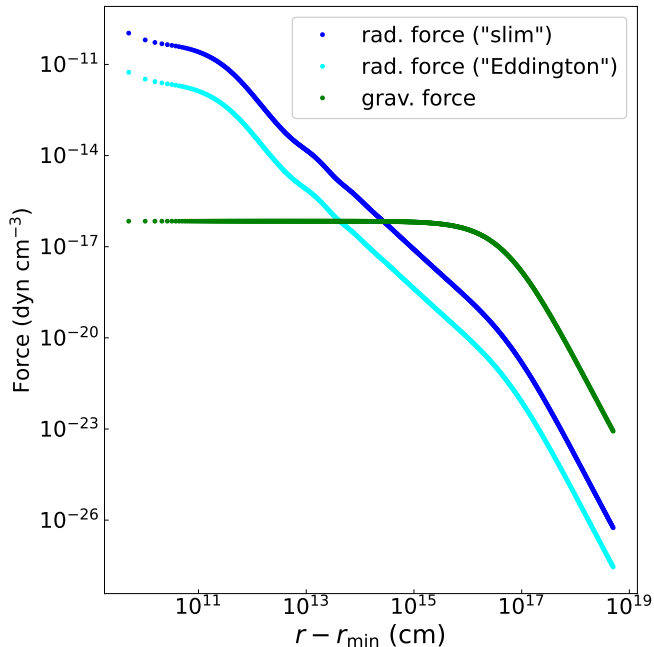


Figure 1: Radial profiles of the Ly α radiation force and gravity (green) for $M_{\text{BH}} = 10^{5.5} M_{\odot}, n_{\infty} = 10^5 \text{ cm}^{-3}$. The horizontal axis shows the radial coordinate measured from $r = r_{\text{min}}$, while the vertical axis shows the force exerted on the gas per unit volume in cgs unit. The blue (cyan) points show the radiation force in the "slim" ("Eddington", respectively) model.

radius) of the region where the radiation force exceeds gravity is larger. In the case with the smallest optical depth in this study ($M_{\text{BH}}, n_{\infty}) = (10^4 M_{\odot}, 10^4 \text{ cm}^{-3})$, the radiation force in the "slim" case overwhelms gravity throughout the entire computational domain.

3.2 Force multiplier

Fig.2 depicts the relationship between the total optical depth at the Ly α line center across the entire computational domain and the force multiplier M_{F}^1 , which is defined as:

$$M_{\text{F}} = \frac{c}{L_{\text{Ly}\alpha}} \int f_{\text{rad}} dV. \quad (20)$$

We can observe that the force multiplier remains almost independent of the optical depth, maintaining a constant value of $M_{\text{F}} \approx 130$. The reason for this is primarily attributed to the effect of the two-photon decay, rather than the Doppler shift caused by the velocity and its gradient.

To illustrate the reason, we examine the following two cases. The first is the case of a static, homogeneous hydrogen medium where Ly α photons are assumed not to be destroyed. In this case, M_{F} can be analytically described² as (Tomaselli & Ferrara, 2021)

¹It is worth noting that the force multiplier is sometimes defined as the ratio between the actual radiation force and the radiation force considering only Thomson opacity (Castor et al., 1975). However, the definition used here is different from it.

²We use the definition $\text{arctanh}(x) = \frac{1}{2} \ln\left(\frac{1+x}{1-x}\right)$.

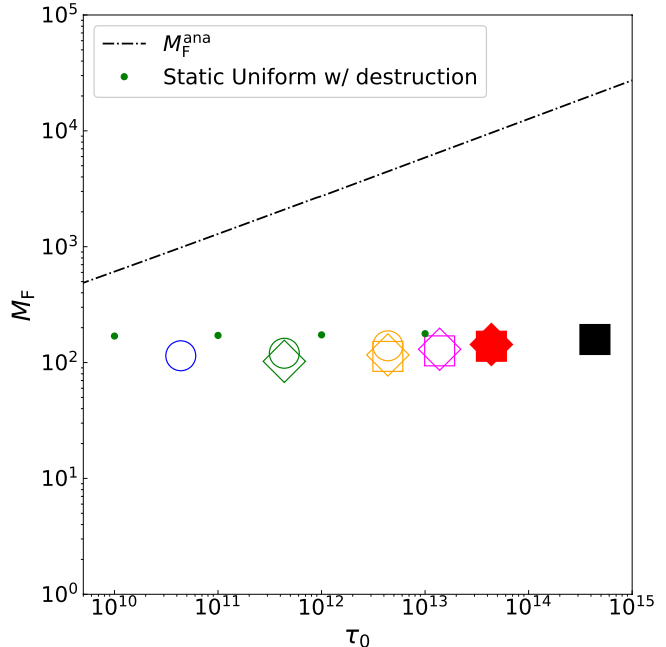


Figure 2: The relationship between the optical depth of the entire system at the Ly α line center and the force multiplier of the Ly α radiation. The same symbols represent models with the same number density n_{∞} (the model with $n_{\infty} = 10^4, 10^5, 10^6 \text{ cm}^{-3}$ corresponding to the circle, diamond, square symbols, respectively) and the same colors of the symbols indicate the models with the same optical depth through the system, τ_0 . Whether or not the symbol is filled with color indicates whether the relation $F_{\text{rad}} < F_{\text{grav}}$ (refer also to the description around Eq.23) is satisfied or not. The black dashed line represents the analytical solution for the case of static homogeneous hydrogen gas, $M_{\text{F}}^{\text{ana}}$, given by Eq.22. The green points show the results of the computation of static homogeneous gas with destruction processes.

$$M_{\text{F}}^{\text{ana}}(\tau_0) = \frac{4}{\pi} \sqrt{\frac{2}{3}} \int_{-\infty}^{\infty} \text{arctanh}(e^{-\pi|\sigma(x)|/\tau_0}) dx, \quad (21)$$

where $\sigma(x) = \int_0^x \sqrt{2/3}/H(y, a) dy$. In the limit of a large optical depth, this equation can be approximated as:

$$M_{\text{F}}^{\text{ana}}(\tau_0) \approx 3.51(a\tau_0)^{1/3} = 610 \left(\frac{\tau_0}{10^{10}}\right)^{1/3} \left(\frac{T}{10^4 \text{K}}\right)^{-1/6}, \quad (22)$$

which is also represented in Fig.2 by the black dot-dashed line. The second is the case where destruction of Ly α photons are taken into consideration in a static homogeneous hydrogen gas. The results of numerical calculation are shown by the green points. It is observed that the resulting M_{F} is considerably smaller than that of the first case, closely agreeing with the outcomes of our present study. This indicates that the radiation force diminishes and M_{F} becomes constant with τ_0 , not due to the velocity gradient, but owing to photon destruction. This fact can be understood as follows: Ly α photons undergo numerous scattering and vanish when traveling the distance equivalent to the mean free path for the photon destruction process. Consequently, the Ly α radiation force effectively work only within the extent that Ly α photons

can penetrate, and it becomes approximately constant regardless of τ_0 , even when the optical depth of the system is considerably large. Since the region penetrated by Ly α photons is extremely narrow, the velocity change within the region is small. Therefore, the effect of the velocity field on M_F is negligibly small (see Appendix B for more details). Note that the constancy of the force multiplier holds true only when the gas number density n_∞ is between 10^8 cm^{-3} and 10^{12} cm^{-3} as mentioned in Appendix B. It is also noteworthy that the properties of M_F discussed in this subsection are independent of $L_{\text{Ly}\alpha}$. This is because the radiation force, f_{rad} , is proportional to $L_{\text{Ly}\alpha}$ via E_{x_0} (see Eq. 19).

3.3 Comparison between Ly α radiation force and gravity

Fig.3 summarizes the possibility of the supercritical accretion on the n_∞ - M_{BH} plane for the "slim" models. The filled symbols show the models where the super-Eddington accretion is possible as $F_{\text{grav}} > F_{\text{rad}}$. Here, F_{grav} and F_{rad} are gravitational and radiation forces integrated across the entire simulation domain, defined as follows:

$$F_{\text{grav}} = 4\pi \int_{r_{\text{min}}}^{r_{\text{max}}} G\rho M_{\text{BH}} dr, \quad (23)$$

$$F_{\text{rad}} = \int_{r_{\text{min}}}^{r_{\text{max}}} f_{\text{rad}} 4\pi r^2 dr = \frac{M_F}{c} L_{\text{Ly}\alpha}. \quad (24)$$

The radiation force F_{rad} is proportional to the force multiplier M_F and the Ly α luminosity. The latter is given by the product of the Eddington luminosity and a factor that is either fixed to 0.1 for the "Eddington" case or depends on $n_\infty M_{\text{BH}}$ from Eqs.13 and 18 for the "slim" case.

This figure shows that the Ly α radiation force elevates the lower limit of $n_\infty M_{\text{BH}}$ for realizing super-Eddington accretion. The grey area represents the parameter range where the super-Eddington accretion is unattainable even in the absence of the Ly α radiation force (Inayoshi et al., 2016; Sakurai et al., 2016)³. By incorporating the Ly α radiation force, the region of non-supercritical accretion expands into the shaded area. Our calculations confirm that the seven models within the shadow region are incapable of supporting super-Eddington accretion.

The boundary of the shaded area and the unshaded region (super-Eddington are) can be derived through analytical considerations. Assuming the density profile of the Bondi accretion at the inner limit, $n(r) = n_\infty (r/r_B)^{-3/2}$, the gravitational force F_{grav} (Eq.23) can be written as

$$F_{\text{grav}} \simeq 4.2 \frac{L_{\text{Edd}}}{c} \left(\frac{n_\infty}{10^5 \text{ cm}^{-3}} \right) \left(\frac{M_{\text{BH}}}{10^4 M_\odot} \right) \left(\frac{T}{10^4 \text{ K}} \right)^{-1} \left(\frac{r_{\text{min}}}{10^{-3} r_B} \right)^{-1/2} \quad (25)$$

³Note that Toyouchi et al. (2019) derives the relation where the required value for $n_\infty M_{\text{BH}}$ is one order of magnitude larger than the previous studies by considering the pressure balance on the boundary of HII region, but without the Ly α radiation.

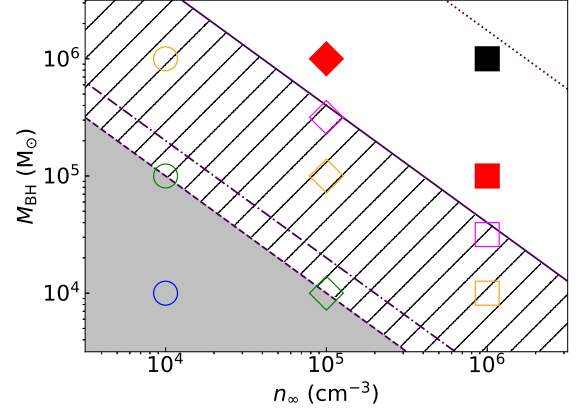


Figure 3: The feasibility of the supercritical accretion in all models within the "slim" category. Each symbol shows the result of the computation for a specific model, with its color corresponding to the model with the different parameter set (M_{BH}, n_∞). Filled symbols show the models where gravity prevails over radiation, expressed as $F_{\text{grav}} > F_{\text{rad}}$, while unfilled symbols show the opposite cases. The lines delineate the boundaries where the supercritical accretion can be achieved, with $(n_\infty/10^5 \text{ cm}^{-3})(M_{\text{BH}}/10^4 M_\odot) = 1$ (dashed), 2 (dot-dashed), 40 (solid) and 1500 (dotted). The dashed line corresponds to the results in Inayoshi et al. (2016); Sakurai et al. (2016). The dot-dashed and solid lines correspond to the results of the simple formula Eq.26 with $r_{\text{min}} = 10^{-3} r_B$, applied for the "Eddington" and "slim" models, respectively. The dotted line corresponds to that with $r_{\text{min}} = r_B$, applied for the "slim" model.

and thus the ratio of F_{rad} and F_{grav} can be expressed as

$$\frac{F_{\text{rad}}}{F_{\text{grav}}} \sim 2 \left(\frac{n_\infty}{10^5 \text{ cm}^{-3}} \right)^{-1} \left(\frac{M_{\text{BH}}}{10^4 M_\odot} \right)^{-1} \times \left(\frac{M_F}{100} \right) \left(\frac{L_{\text{Ly}\alpha}}{0.1 L_{\text{Edd}}} \right) \left(\frac{r_{\text{min}}}{10^{-3} r_B} \right)^{1/2} \left(\frac{T}{10^4 \text{ K}} \right). \quad (26)$$

The force multiplier, M_F , is approximately 100 in the parameter sets employed in our study (see also fig.2), allowing us to deduce $(n_\infty/10^5 \text{ cm}^{-3})(M_{\text{BH}}/10^4 M_\odot) = 40$ from $F_{\text{rad}} = F_{\text{grav}}$ for the "slim" case. Consequently, super-Eddington accretion occurs when the gas density and the BH mass satisfy the condition $(n_\infty/10^5 \text{ cm}^{-3})(M_{\text{BH}}/10^4 M_\odot) \gtrsim 40$ for the "slim" case. A similar argument yields the condition $(n_\infty/10^5 \text{ cm}^{-3})(M_{\text{BH}}/10^4 M_\odot) \gtrsim 2$ for the "Eddington" case. Note that, in the "slim" case, the condition is more stringent because of the luminosity exceeding the Eddington limit, resulting in a stronger radiation force.

The reason why the relation depends only on $M_{\text{BH}} n_\infty$ even in the "slim" case is attributed to the fact that the ratio $L_{\text{Ly}\alpha}/L_{\text{Edd}}$ depends only on $\dot{M}_B/(L_{\text{Edd}}/c^2)$, which is proportional to $n_\infty M_{\text{BH}}$ (see Eqs.13 and 18). The boundary drawn under this assumption agrees with our results. It should be noted that the analytical description of $F_{\text{rad}}/F_{\text{grav}}$ includes the inner boundary radius, r_{min} , which is fixed to $r_{\text{min}} = 10^{-3} r_B$ in our model but nearly unknown in realistic cases. If the inner boundary radius r_{min} , corresponding to the HII region radius, increases, the gravitational force becomes weaker in the innermost region, facilitating the dominance

of the radiation force over gravity. According to the simulation of the super-Eddington flow in Inayoshi et al. (2016), the size of the HII region in the early phase is similar to the Bondi radius. At this stage, Ly α radiation becomes more important. Under the condition of $r_{\min} \sim r_B$, the required value of $n_{\infty,5} M_{\text{BH},4}$ to realize the super-Eddington accretion becomes about thirty times larger than that with $r_{\min} = 10^{-3} r_B$ and reaches ~ 1500 for the "slim" case.

4 Summary and Discussion

To assess the impact of the Ly α radiation force on Bondi-like super-Eddington accretion flows, as previously discussed in Inayoshi et al. (2016); Sakurai et al. (2016), we have calculated the radiation field of Ly α photons using the diffusion approximation. Our calculations take into account the destruction processes, such as two photon decay and collisional de-excitation. We have explored the parameter range of $10^4 \leq M_{\text{BH}} [M_{\odot}] \leq 10^6$ and $10^4 \leq n_{\infty} [\text{cm}^{-3}] \leq 10^6$. Our model supposes that the computational domain is filled with an isothermal Bondi flow of HI gas and that Ly α photons are injected through the inner boundary, considering that the gas located closer to the center than the inner boundary is ionized by the UV photons emitted from the black hole accretion disk. Below we summarize our key findings:

- We have found that the Ly α radiation force becomes much stronger than the gravity in the immediate vicinity of the inner boundary. However, as distance increases, the influence of the radiation force diminishes, and gravity becomes the predominant force at larger distances. This implies that the Ly α radiation force effectively hinders inflow motion solely within the narrow region of atomic hydrogen (HI) gas immediately outside the ionized HII region.
- The pronounced strength of the Ly α radiation force is attributed to resonance scatterings. Despite undergoing numerous scatterings, Ly α photons are ultimately annihilated by destructive processes such as two-photon decay and collisional de-excitation. Given that many Ly α photons penetrate slightly from the inner boundary and are subsequently destroyed, the Ly α radiation force experiences enhancement only near the innermost edge of the HI region. The force multiplier remains constant around 130 and does not increase with the optical thickness of the system.
- The strong Ly α radiation force necessitates a higher value of $n_{\infty} M_{\text{BH}}$ to realize super-Eddington accretion. Specifically, when the luminosity of the black hole accretion disk follows the prediction of the slim accretion disk, the condition for realizing super-Eddington accretion is given by $(n_{\infty}/10^5 \text{cm}^{-3})(M_{\text{BH}}/10^4 M_{\odot}) \gtrsim 40$, in contrast to $(n_{\infty}/10^5 \text{cm}^{-3})(M_{\text{BH}}/10^4 M_{\odot}) \gtrsim 1$ when the Ly α radiation force is not taken into account (Inayoshi et al., 2016). If the luminosity of the disk is limited by the Eddington luminosity, the condition is relaxed $(n_{\infty}/10^5 \text{cm}^{-3})(M_{\text{BH}}/10^4 M_{\odot}) \gtrsim 2$.

Even if we relax the diffusion approximation employed in the present study, the main results would remain largely unaltered. The diffusion approximation is valid only if the mean free path of the photon remains considerably smaller than the dimensions of the system. The Doppler effect induces deviations in the frequency of Ly α photons from the line center value, leading to an enhancement of the mean free path. Consequently, the accuracy of calculations diminishes as the velocity gradient increases. Indeed, the diffusion approximation reproduces the spectrum of the Hubble flow successfully in cases with small velocity gradient, while it fails in cases with large velocity gradient (see Appendix A for more detail). In the case of the Bondi accretion flow, treated in our study, most Ly α photons are destructed before the velocity gradient becomes influential (Appendix B). Although some photons manage to survive destruction and their mean free path can be comparable to or even greater than the size of the system, the radiation force exerted by such photons is not significantly large. In instances involving low density or pronounced velocity gradients, a relaxation of the diffusion approximation becomes imperative for more accurate modeling, as discussed in Appendix B.

It is important to note, as mentioned in Sec. 3.3, that the size of HII regions, corresponding to r_{\min} , is not well-defined in realistic cases. In the super-Eddington simulations by Inayoshi et al. (2016), the HII region gradually shrinks over time and eventually vanishes, meaning that the size of the HII region can be arbitrarily small. In more realistic cases, an accretion disk would form inside the centrifugal radius. High-energy radiation from the disk effectively ionizes the surrounding gas, creating an HII region. In this case, the size of the HII region would be comparable to or larger than the centrifugal radius, which is similar to or greater than $\sim 10^{-1} M_{\text{BH},4}$ times the Bondi radius (see Eq. 19 in Sugimura et al. 2018). Recall that the HII region we considered is much smaller than those estimates. As the size of the HII region, r_{\min} , decreases, the ratio $F_{\text{rad}}/F_{\text{grav}}$ also decreases, as shown in Eq. 26, making super-Eddington accretion more likely. In this sense, our estimate of the effect of the Ly α radiation force is conservative. Further investigation into the size of the HII region and the impact of Ly α radiation is awaited, particularly through radiation hydrodynamic simulations that incorporate Ly α radiative transfer.

The destruction of Ly α photons, as demonstrated in the present study, plays an important role in the early universe, but should be more effective in environments with higher metallicity. Assuming that the gas flow setup in this study contains typical astronomical silicate dust, the ratio of the destruction rate by the two-photon decay and the collisional de-excitation to that by dust absorption can be estimated as $\sim 0.5 (T/10^4 \text{K})^{-1/2} (Z/Z_{\odot})^{-1}$, where Z/Z_{\odot} denotes the metallicity relative to solar abundance. This implies that Ly α photons are more effectively eliminated by dust absorption in flows with higher metallicity. It should be noted, however, that in environments with higher metallicity, while the radiation force due to Ly α photons is attenuated, the radiation force due to dust absorption becomes more enhanced.

While the Ly α radiation force is evaluated here for fixed distributions of the density, temperature, and velocity, exploring its time evolution is a crucial aspect for future studies. The Ly α radi-

ation force can dynamically alter the flow structure, thereby influencing its impact on the gas. To unravel whether super-Eddington accretion occurs, it is essential to study the time evolution of radiation fields coupled with fluid dynamics. This necessitates the application of radiation hydrodynamics simulations.

Although the present study assumes spherical symmetry, it is important to consider potential multi-dimensional effects. In cases where the accretion flow exhibits anisotropy, Ly α photons may escape preferentially along directions characterized by lower HI column density, thus reducing the impact of the Ly α radiation force that works to prevent accretion.

It has been reported that multidimensional effects can suppress the decrease in the mass accretion rate (Sugimura et al., 2018; Takeo et al., 2018). The anisotropy in these cases arises from the gas possessing angular momentum and the anisotropic radiation emitted by the super-Eddington accretion flow. Moreover, Takeuchi et al. (2013) have reported that the radiation Rayleigh-Taylor instability induces anisotropic structures resembling gas clumps (see also Takeuchi et al., 2014; Jiang et al., 2013). Undertaking multi-dimensional radiation hydrodynamics simulations emerges as a pivotal consideration for future research.

Acknowledgement

The authors wish to express their cordial gratitude to their most revered mentor, Prof. Masayuki Umemura, the *Pater Patriae* of the Theoretical Astrophysics Group at the University of Tsukuba, for his continual interest, advice, and encouragement. This work is supported by JSPS KAKENHI Grant Numbers JP22KJ0420 (TM), in part by MEXT/JSPS KAKENHI grant numbers 17H04827, 20H04724, 21H04489 (HY), 17H01102, 22H00149 (KO), NAOJ ALMA Scientific Research grant numbers 2019–11A, JST FOREST Program, grant number JP-MJFR202Z, and Astro Biology Center Project research AB041008 (HY).

References

- Adams T. F., 1975, ApJ, 201, 350
- Bogdán Á., et al., 2024, Nature Astronomy, 8, 126
- Castor J. I., Abbott D. C., Klein R. I., 1975, ApJ, 195, 157
- Dijkstra M., 2019, Saas-Fee Advanced Course, 46, 1
- Dijkstra M., Haiman Z., Spaans M., 2006, ApJ, 649, 14
- Drawin H., 1969, Zeitschrift für Physik A Hadrons and nuclei, 225, 483
- Fan X., et al., 2004, AJ, 128, 515
- Haiman Z., 2013, in Wiklind T., Mobasher B., Bromm V., eds, Astrophysics and Space Science Library Vol. 396, The First Galaxies. p. 293 (arXiv:1203.6075), doi:10.1007/978-3-642-32362-1_6
- Inayoshi K., Haiman Z., Ostriker J. P., 2016, MNRAS, 459, 3738
- Inayoshi K., Visbal E., Haiman Z., 2020, ARA&A, 58, 27
- Jiang Y.-F., Davis S. W., Stone J. M., 2013, ApJ, 763, 102
- Jiang Y.-F., Stone J. M., Davis S. W., 2014, ApJ, 796, 106
- Kormendy J., Ho L. C., 2013, ARA&A, 51, 511
- Laursen P., Razoumov A. O., Sommer-Larsen J., 2009, ApJ, 696, 853
- Matsuoka Y., et al., 2018, PASJ, 70, S35
- McKinney J. C., Tchekhovskoy A., Sądowski A., Narayan R., 2014, MNRAS, 441, 3177
- Mihalas D., Mihalas B. W., 1984, Foundations of radiation hydrodynamics
- Milosavljević M., Couch S. M., Bromm V., 2009a, ApJL, 696, L146
- Milosavljević M., Bromm V., Couch S. M., Oh S. P., 2009b, ApJ, 698, 766
- Mortlock D. J., et al., 2011, Nature, 474, 616
- Neufeld D. A., 1990, ApJ, 350, 216
- Ohsuga K., Mineshige S., 2014, Space Sci. Rev., 183, 353
- Ohsuga K., Mori M., Nakamoto T., Mineshige S., 2005, ApJ, 628, 368
- Omukai K., 2001, ApJ, 546, 635
- Park K., Ricotti M., 2011, ApJ, 739, 2
- Park K., Ricotti M., 2012, ApJ, 747, 9
- Park K., Ricotti M., 2013, ApJ, 767, 163
- Sakurai Y., Inayoshi K., Haiman Z., 2016, MNRAS, 461, 4496
- Seaton M. J., 1955, Proceedings of the Physical Society A, 68, 457
- Sądowski A., Narayan R., Tchekhovskoy A., Abarca D., Zhu Y., McKinney J. C., 2015, MNRAS, 447, 49
- Smith A., Safranek-Shrader C., Bromm V., Milosavljević M., 2015, MNRAS, 449, 4336
- Smith A., Bromm V., Loeb A., 2016, MNRAS, 460, 3143
- Sobel’Man I. I., Vainshtein L. A., Yukov E. A., 1995, Excitation of Atoms and Broadening of Spectral Lines
- Sugimura K., Hosokawa T., Yajima H., Omukai K., 2017, MNRAS, 469, 62
- Sugimura K., Hosokawa T., Yajima H., Inayoshi K., Omukai K., 2018, MNRAS, 478, 3961
- Takeo E., Inayoshi K., Ohsuga K., Takahashi H. R., Mineshige S., 2018, MNRAS, 476, 673

- Takeuchi S., Ohsuga K., Mineshige S., 2013, PASJ, 65, 88
- Takeuchi S., Ohsuga K., Mineshige S., 2014, PASJ, 66, 48
- Tomaselli G. M., Ferrara A., 2021, MNRAS, 504, 89
- Toyouchi D., Hosokawa T., Sugimura K., Nakatani R., Kuiper R., 2019, MNRAS, 483, 2031
- Toyouchi D., Inayoshi K., Hosokawa T., Kuiper R., 2021, ApJ, 907, 74
- Volonteri M., 2012, Science, 337, 544
- Watarai K.-y., Fukue J., Takeuchi M., Mineshige S., 2000, PASJ, 52, 133
- Wu X.-B., et al., 2015, Nature, 518, 512
- Yajima H., Ricotti M., Park K., Sugimura K., 2017, ApJ, 846, 3

A Validity of diffusion approximation

Our calculation includes the effect of velocity up to $O(v/c)$, which means the Doppler effect by the velocity and its gradient and the energy loss/gain by the work to/from the fluid are included. To check if these effects are solved correctly in our code, we compare our calculation with the Monte-Carlo calculation in the Hubble flow by Laursen et al. (2009). The velocity field in the Hubble flow is given by

$$v(r) = V_{\max} \frac{r}{R_{\max}} \quad (27)$$

where the parameters R_{\max} and V_{\max} are the radius of the outer boundary and the maximum velocity, respectively. The gas is distributed homogeneously with a column density of $2 \times 10^{20} \text{ cm}^{-2}$ and is isothermal with the temperature of 10^4 K . Fig.4 shows the frequency dependence of resulting radiation energy at $r = R_{\max}$, with the maximum velocity V_{\max} varying from 0 km s^{-1} to 2000 km s^{-1} . Our calculations nicely reproduce the results of the previous study in the case of $V_{\max} = 0, 20, 200 \text{ km s}^{-1}$. However, our results deviate from the correct answer in the case of very large velocity, $V_{\max} = 2000 \text{ km s}^{-1}$. This is because that the diffusion approximation is invalid in an optically thin medium. Due to the Doppler shifting by the large velocity gradient, most photons immediately go out of the Ly α line center and the mean free path of photons is dramatically increased. Then, the diffusion approximation breaks down. Our calculation cannot correctly treat such a large velocity situation.

The limit of the approximation can be estimated by comparing the energy shift by the resonance scattering with that by the velocity gradient. The shift by the velocity gradient is $\sim V_{\max}/v_{\text{th}}$ while that by resonance scattering is $\sim (a\tau_0)^{1/3} \approx 13(N_{\text{HI}}/10^{20} \text{ cm}^{-2})^{1/3}$ (see Eq.30) when photons traveling through the whole system, where $v_{\text{th}} \approx 13 \times (T/10^4 \text{ K})^{1/2} \text{ km/s}$ and $a = 4.7 \times 10^{-4} T_4^{-1/2}$, respectively. Therefore, when the velocity is much greater than $\sim 200 \text{ km s}^{-1}$, system becomes effectively very optically thin and the diffusion approximation is no longer valid. This argument is consistent with the results of our test calculations. It should

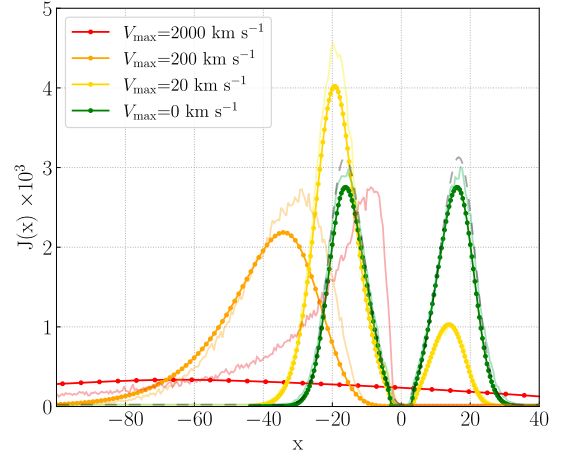


Figure 4: The emergent spectrum from homogeneous isothermal HI gas with the temperature $T = 10^4 \text{ K}$, the Hubble flow velocity $v(r)$ in Eq. 27 and the column density $N_{\text{HI}} = 2 \times 10^{20} \text{ cm}^{-2}$. Curves with different colors show results of the models with different maximum velocity V_{\max} . The thin lines show the results of Laursen et al. (2009), with their colors corresponding to the models with the same V_{\max} as our results. The thin dashed black line is drawn by the analytical formula derived in Dijkstra et al. (2006).

be noted that the diffusion approximation remains valid in the present study, even when the velocity reaches $\sim 1000 \text{ km/s}$ in the innermost region of the Bondi flow, since the column density of the system is much greater than in this test calculation. Consequently, the acceptable maximum velocity to maintain the validity of the diffusion approximation is also $\gtrsim 1000 \text{ km/s}$.

B Detailed comparison with static homogeneous gas with destruction process

We discuss the reason why the force multiplier is almost constant regardless of optical depth when the destruction process is effective. Fig.5 shows the force multiplier in the static spherical homogeneous hydrogen gas with $T = 10^4 \text{ K}$, $x_e = 10^{-4}$ and with the destruction process and with the different n_{∞} as a function of the optical depth τ_0 . We can see clearly, in this figure, the saturation of the force multiplier, and also that the terminal values depend on the number density, n_{∞} .

Here, we confirm this trend through a simple analysis. The destruction of Ly α photons occurs when the number of scatterings approximately reaches $\sim 1/p_{\text{dest}}$. Therefore, in the case that the optical depth of the system, τ_0 , is much larger than $1/p_{\text{dest}}$, almost all Ly α photons are destroyed in the system. Consequently, the force multiplier is independent of τ_0 but is capped at $1/p_{\text{dest}}$.⁴

In contrast, for $\tau_0 \ll 1/p_{\text{dest}}$, the destruction process is negligible and thus the force multiplier can be analytically obtained as $M_F^{\text{ana}}(\tau_0)$. Therefore, the relationship between τ_0 and M_F in the

⁴In a random walk caused by resonant scattering, the distance is proportional to the number of scatterings, as noted by Dijkstra 2019. Photons escape the medium more easily during resonant scattering because the cross-section decreases as the photon frequency shifts away from the line center with an increasing number of scatterings.

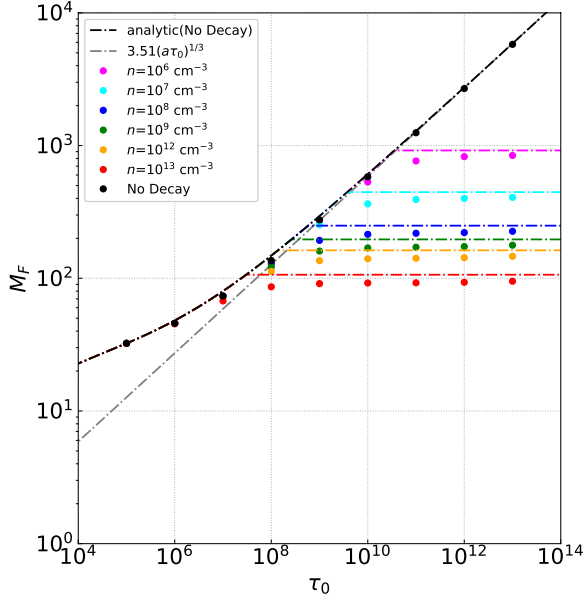


Figure 5: The force multiplier in a static homogeneous gas with the destruction process. Points in various colors, excluding the black ones, represent model results with the destruction process at different number densities, denoted as n . The black points depict the outcomes of calculations for a static homogeneous gas without the destruction process. The black dot-dashed line represents the analytical solution of the homogeneous model without the destruction process, given in Eq.(21), while the grey dot-dashed line presents its approximated formula, proportional to $\tau_0^{1/3}$. The dot-dashed horizontal lines in various colors indicate the saturated values of the force multiplier at different number densities, as given by Eq.28.

presence of the destruction process is given by

$$M_F(\tau_0, n_H) = \min\left(M_F^{\text{ana}}(\tau_0), M_F^{\text{ana}}(1/p_{\text{dest}}(n_H))\right). \quad (28)$$

We now provide an overview of the behavior of p_{dest} by introducing an approximation:

$$p_{\text{dest}} \equiv \bar{p}_{\text{dest}} f(n_H) \approx \bar{p}_{\text{dest}} \left(\frac{n_H}{n_H + n_{\text{H,crit1}}} + \frac{n_H}{n_{\text{H,crit2}}} \right), \quad (29)$$

where $\bar{p}_{\text{dest}} \equiv A_{2s1s}/(3A_{2p1s}) \approx 4.39 \times 10^{-9}$ is the typical value of p_{dest} . The critical values $n_{\text{H,crit1}}$ and $n_{\text{H,crit2}}$ are defined as $n_{\text{H,crit1}} \equiv n_H A_{2s1s}/C_{2s2p} \approx 1.55 \times 10^8 (x_e/10^{-4})^{-1} \text{ cm}^{-3}$ and $n_{\text{H,crit2}} \equiv A_{2s1s}/((x_e/10^{-4})\gamma_{21}(\text{e}) + \gamma_{21}(\text{H}))/4 \approx 1.75 \times 10^{12}/((x_e/10^{-4}) + 0.145) \text{ cm}^{-3}$, respectively, determine the n_{H} -dependence of p_{dest} . In the limit of large τ_0 , Eq.28 can be rewritten as

$$M_F(\infty, n_H) \approx 150 f(n_H)^{-1/3} T_4^{-1/6}. \quad (30)$$

Static homogeneous models reproduce the limit in Fig.5, where the force multiplier of each models (colored circles) converges to the value of Eq.30 (colored dot-dashed lines) in the limit of the large optical depth. The function $f(n_H) \equiv p_{\text{dest}}/\bar{p}_{\text{dest}}$ can be

approximated as

$$f(n_H) \approx \begin{cases} \frac{n_H}{n_{\text{H,crit1}}} & \text{if } n_H < n_{\text{H,crit1}} \\ 1 & \text{if } n_{\text{H,crit1}} < n_H < n_{\text{H,crit2}} \\ \frac{n_H}{n_{\text{H,crit2}}} & \text{if } n_H > n_{\text{H,crit2}} \end{cases}. \quad (31)$$

The approximation in Eq.29 with Eq.31 has an accuracy up to 10^{-2} in relative error. Using Eq.31, Eq.30 shows that in the number density range between 10^8 cm^{-3} and 10^{12} cm^{-3} , the terminal force multiplier is almost constant, as long as the gas temperature does not change. In other density ranges, it exhibits a weak dependency on n_{H} , proportional to $n_{\text{H}}^{1/3}$. This can explain the trend in the region with large τ_0 shown in Fig.5, where force multiplier depends on $n[\text{cm}^{-3}]$ in the range of 10^6 to 10^8 , but not in the range of 10^8 to 10^{13} . Therefore, the force multiplier remains almost constant around 130 in our model.

In Section 3.2, we emphasized that the velocity gradient is less significant than the destruction process. The reason for this is that Ly α photons penetrate only in a narrow region at the innermost region ($r - r_{\text{min}} < r_{\text{min}}$), where the velocity changes only slightly. The distance at which the velocity gradient becomes non-negligible is given by comparing the frequency shift induced by the velocity gradient with that caused by the thermal velocity dispersion, $\Delta r_{\text{vg}} = v_{\text{th}} |dv/dr|^{-1}$.

The velocity distribution is considered as $v(r) \sim v_{\text{th}}(r/r_B)^{-1/2}$ in the innermost region, so we have

$$\Delta r_{\text{vg}} \sim 3 \times 10^{-5} r_B, \quad (32)$$

where we use $r = 10^{-3} r_B (= r_{\text{min}})$. On the other hand, the typical distance, Δr_{pd} , that Ly α photons can penetrate corresponds to the length at which the optical depth of the line-center is $1/p_{\text{dest}}$. Thus, Δr_{pd} at the innermost region is evaluated as

$$\Delta r_{\text{pd}} \sim 2 \times p_{\text{dest}}^{-1} \tau_0^{-1} r_{\text{min}} \simeq 4 \times 10^5 \tau_0^{-1} r_B, \quad (33)$$

which is derived from comparing the optical depth from r_{min} to $r_{\text{min}} + \Delta r_{\text{pd}}$ with $\tau^* = 1/p_{\text{dest}}$ where we assume $n_{\text{H}} \propto r^{-3/2}$ and $p_{\text{dest}} \sim 5.0 \times 10^{-9}$. In our models, $\Delta r_{\text{vg}} \gg \Delta r_{\text{pd}}$ holds since the optical depth, τ_0 , is between 10^{10} and 10^{15} . Consequently, the velocity gradient effect can be negligible.